

A study on load-deflection behavior of two-span continuous concrete beams reinforced with GFRP and steel bars

Ismail Unsal^{1a}, Serkan Tokgoz^{2b}, Ismail H. Cagatay^{1b} and Cengiz Dundar^{*1}

¹Department of Civil Engineering, Cukurova University, 01330 Adana, Turkey

²Department of Civil Engineering, Adana Science and Technology University, 01180 Adana, Turkey

(Received January 28, 2017, Revised May 24, 2017, Accepted May 25, 2017)

Abstract. Continuous concrete beams are commonly used as structural members in the reinforced concrete constructions. The use of fiber reinforced polymer (FRP) bars provide attractive solutions for these structures particularly for gaining corrosion resistance. This paper presents experimental results of eight two-span continuous concrete beams; two of them reinforced with pure glass fiber reinforced polymer (GFRP) bars and six of them reinforced with combinations of GFRP and steel bars. The continuous beams were tested under monotonically applied loading condition. The experimental load-deflection behavior and failure mode of the continuous beams were examined. In addition, the continuous beams were analyzed with a numerical method to predict the load-deflection curves and to compare them with the experimental results. Results show that there is a good agreement between the experimental and the theoretical load-deflection curves of continuous beams reinforced with pure GFRP bars and combinations of GFRP and steel bars.

Keywords: concrete; glass fiber reinforced polymer (GFRP); continuous beam; load-deflection; stress-strain

1. Introduction

Fiber reinforced polymer (FRP) bars are increasingly used in the structures due to their advantages, such as high corrosion resistance, high longitudinal strength capacity, low weight to strength ratio and non-conductivity (Zhao and Zhang 2007, Dundar *et al.* 2015). The main types of fibers used in the constructional members are glass fiber, carbon fiber, basalt fiber and aramid fiber. The primary disadvantage of the fiber material is its brittle behavior. It is known that, fiber material exhibits linear elastic mechanical behavior up to its rupture without yielding. Ductility capacity of reinforced concrete beams can be improved with the use of combinations of FRP and conventional steel reinforcement. FRP material provides high strength capacity and steel reinforcement ensures significant ductility feature (Qin *et al.* 2017).

A number of studies were conducted on concrete beams reinforced with fiber reinforced polymer (FRP) bars. Flexural behavior of FRP reinforced concrete beams has been examined extensively based on several design approaches in terms of various parameters such as load carrying capacity, deformability, serviceability, deflection, crack propagation, moment redistribution, failure mode, reinforcement arrangements and bond (Bischoff 2007, Kara and Ashour 2012, Kara *et al.* 2013, Lou *et al.* 2015, Maranan *et al.* 2015, Zhang *et al.* 2015, Adam *et al.* 2015,

Kara 2016, Goldstone *et al.* 2016, Mohamed *et al.* 2016, Elgabbas *et al.* 2016, Gribniak *et al.* 2016). Thomas and Ramadass (2015) proposed a model for the prediction of shear strength of beams reinforced with FRP bars.

Elamary and Abd-Elwahab (2016) conducted an analytical study using finite element model to simulate the behavior of beam reinforced with glass fiber reinforced polymer (GFRP) and/or steel bars. Qu *et al.* (2009) performed experimental and analytical analysis to describe the flexural performance of GFRP and steel reinforced concrete beams. Qin *et al.* (2017) investigated the effect of hybrid reinforcement ratio on the flexural performance of concrete beams using three dimensional finite element models. The tested specimens were simply supported and subjected to a point load applied at midspan. Yinghao and Yong (2013) investigated the influence of combinations of GFRP and steel bar arrangement on the flexural behavior of high strength concrete beams. The beams were simply supported and subjected to four-point bending test. Refai *et al.* (2015) studied on the GFRP and steel reinforced concrete beams to describe the structural behavior in terms of load carrying capacity, deformability and failure modes. Simply supported specimens were tested under four-point bending load condition. Kara *et al.* (2015) presented a numerical method for estimating the curvature, deflection and moment capacity of simply supported hybrid FRP-steel reinforced concrete beams subjected to four point bending load. Bencardino *et al.* (2016) conducted a numerical analysis of concrete beams reinforced with steel bars, and combinations of FRP and steel bars to determine the ultimate loads and analytical failure modes. Mazaheripour *et al.* (2016) investigated the deflection and cracking behavior of I-shaped cross-sectional beams of steel fiber reinforced self-compacting concrete (SFRSCC) reinforced

*Corresponding author, Professor

E-mail: dundar@cu.edu.tr

^aPh.D.

^bProfessor

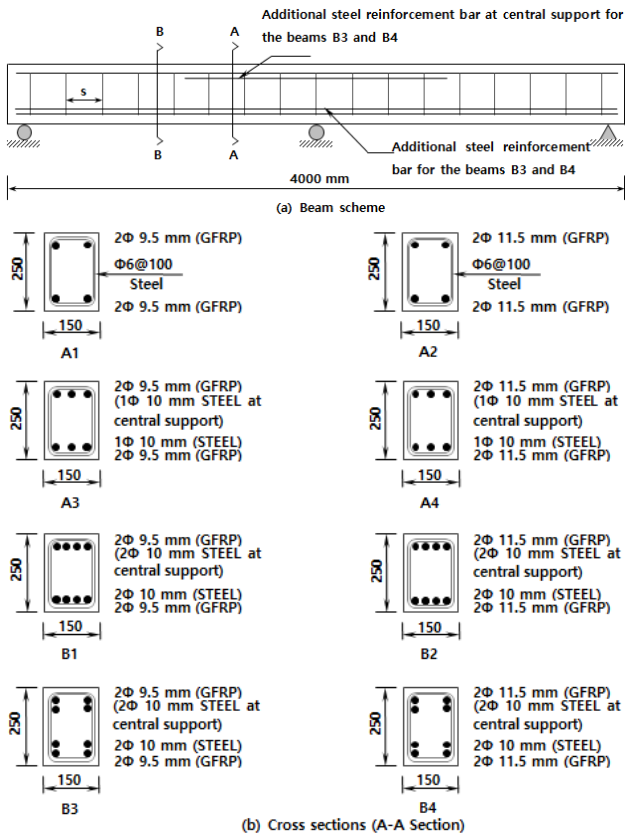


Fig. 1 Continuously supported beams: Beam scheme (a); Cross sections (b)

in flexure with hybrid prestressed steel strand and GFRP bars. The beams were simply supported and subjected to four-point bending test under monotonic and fatigue loading conditions. These studies have led to the development of several standards and guidelines such as CSA S806-12 (2012) and ACI 440.1R-15 (2015). On the other hand, limited experimental researches have been conducted to examine the behavior of continuous concrete beams reinforced with combination of FRP and steel bars.

The objective of this study is to examine the experimental and theoretical load-deflection behavior of two-span continuous concrete beams reinforced with pure GFRP bars and combinations of GFRP and steel bars. These beams were constructed and tested under monotonically applied midspan loads. The load-deflection behavior and failure mode of the specimens were observed in the study. In addition, a theoretical method previously presented in Tanrikulu *et al.* (2000), Kara and Dundar (2012) and Dundar *et al.* (2015) was modified to perform the analysis of continuous concrete beams reinforced with combinations of FRP and steel bars. The tested beams were analyzed based on the numerical method in the study.

2. Experimental program

2.1 Test specimens

Experimental study was conducted on a total of eight



Fig. 2 GFRP bars (9.5 and 11.5 mm in diameter)

two-span continuous concrete beams. The specimens were prepared into two batches, designated as A and B. The beams had 250 mm in depth, 150 mm in width rectangular cross section, and 4000 mm in length. In each series, beams were designed with different longitudinal reinforcement configurations. The specimens were consisted of 9.5 mm and 11.5 mm in diameter GFRP bars. In addition to GFRP bars, 10 mm in diameter conventional steel bars were used for the beams reinforced with combination of GFRP and steel bars. All specimens were confined with 6 mm in diameter lateral reinforcement at spacing of 100 mm. A 25 mm concrete cover was provided for the beams. Specimens A1 and A2 were designed as pure GFRP reinforced beams whereas the other specimens were designed as combinations of GFRP and steel bars. The details of the cross section and reinforcement configuration of the specimens are given in Fig. 1. Clear distance of 30 mm was provided between the inner layer of steel and outer layer of GFRP reinforcement in B3 and B4 specimens. The reinforcement ratio of steel to GFRP (ρ_{ratio}) and details of continuously supported beams are given in Table 1.

The concrete material was manufactured with Portland CEM II A-S 42.5 R type cement content, tap water, clean gravel with maximum size of 22.4 mm and 16 mm for specimens in group A and B, respectively. The concrete composition of the beams is presented in Table 2.

Ribbed surface GFRP bars of 9.5 and 11.5 mm in diameter were used in the experimental study (Fig. 2). Mechanical properties of GFRP bars were provided by the manufacturer (FiReP[®]) as 50 GPa for tensile modulus of elasticity, 1000 MPa for ultimate tensile stress and 2% for ultimate strain.

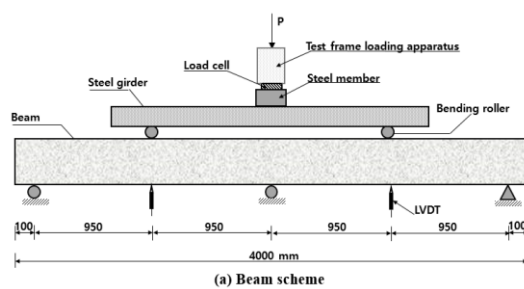
The beams were manufactured in the Structural Laboratory at Cukurova University in Adana, Turkey. The specimens were compacted by using a poker vibrator. Seven control standard cylinder specimens (150 mm in diameter and 300 mm in length) and two beams (100 mm in width, 100 mm in height and 500 mm in length) were cast from concrete mixture to determine the mechanical properties of concrete. The control cylinder specimens were uniaxially tested to determine the concrete compressive strength of beams. The average compressive strength of concrete for groups A and B were 47.7 MPa and 43.1 MPa, respectively. The average flexural tensile strength of concrete for groups A and B were 6.28 MPa and 6.37 MPa, respectively. The size effect of gravel has been neglected in the study.

2.2 Test setup

The continuous beams were supported with two spans. Two linear variable displacement transducers (LVDTs) were applied at midspan of the beams to determine the vertical displacements. A 500 kN capacity load cell was used to

Table 1 Details of two-span continuous beams tested by the authors

Specimen Notation	Location	Section A-A			Section B-B			ρ_{ratio}
		Reinforcement	Material	f_{fu} or f_y (MPa)	Reinforcement	Material	f_{fu} or f_y (MPa)	
A1	Bottom	2Ø9.5	GFRP	1000	2Ø9.5	GFRP	1000	0
	Top	2Ø9.5	GFRP	1000	2Ø9.5	GFRP	1000	-
A2	Bottom	2Ø11.5	GFRP	1000	2Ø11.5	GFRP	1000	0
	Top	2Ø11.5	GFRP	1000	2Ø11.5	GFRP	1000	-
A3	Bottom	2Ø9.5	GFRP	1000	2Ø9.5	GFRP	1000	0.55
		1Ø10	Steel	550	1Ø10	Steel	550	
	Top	2Ø9.5	GFRP	1000	2Ø9.5	GFRP	1000	-
A4	Bottom	2Ø11.5	GFRP	1000	2Ø11.5	GFRP	1000	0.38
		1Ø10	Steel	550	1Ø10	Steel	550	
	Top	2Ø11.5	GFRP	1000	2Ø11.5	GFRP	1000	-
B1	Bottom	2Ø9.5	GFRP	1000	2Ø9.5	GFRP	1000	1.11
		2Ø10	Steel	550	2Ø10	Steel	550	
	Top	2Ø9.5	GFRP	1000	2Ø9.5	GFRP	1000	-
B2	Bottom	2Ø11.5	GFRP	1000	2Ø11.5	GFRP	1000	0.76
		2Ø10	Steel	550	2Ø10	Steel	550	
	Top	2Ø11.5	GFRP	1000	2Ø11.5	GFRP	1000	-
B3	Bottom (outer)	2Ø9.5	GFRP	1000	2Ø9.5	GFRP	1000	1.11
	Bottom (inner)	2Ø10	Steel	550	2Ø10	Steel	550	
	Top (outer)	2Ø9.5	GFRP	1000	2Ø9.5	GFRP	1000	-
	Top (inner)	2Ø10	Steel	550	-	-	-	
B4	Bottom (outer)	2Ø11.5	GFRP	1000	2Ø11.5	GFRP	1000	0.76
	Bottom (inner)	2Ø10	Steel	550	2Ø10	Steel	550	
	Top (outer)	2Ø11.5	GFRP	1000	2Ø11.5	GFRP	1000	-
	Top (inner)	2Ø10	Steel	550	-	-	-	



(b) Beam view

Fig. 3 Test setup and instrumentations: Beam scheme (a); Beam view (b)

Table 2 Concrete composition of beams

Specimen Group	Gravel (kg/m ³)	Sand (kg/m ³)	Cement (kg/m ³)	Water (kg/m ³)
A	919	933	273	166.5
B	813	1055	340	170.8

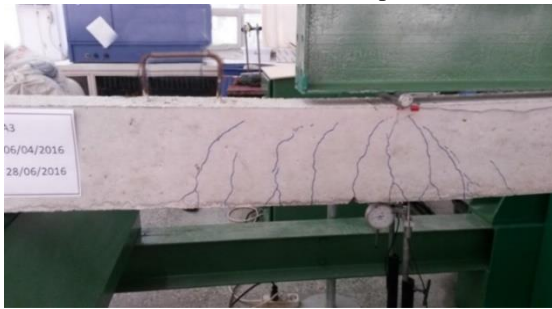
measure the applied load. The applied load and displacement values were recorded by a data acquisition system. Two-span continuous beams had two equal spans with 1900 mm length. Each specimen was supported on a roller and a pinned support at the ends and a roller support on mid-point. The specimens were tested by a 200 kN capacity universal testing machine. The load was applied at each midspan with a rate of 1 kN/s until failure. At each load increment, the applied load and corresponding displacement values were recorded. The typical continuous beam test setup is illustrated in Fig. 3.

2.3 Test result

The applied load, midspan deflections, and crack



(a) Beam A1 left midspan



(b) Beam A3 left midspan

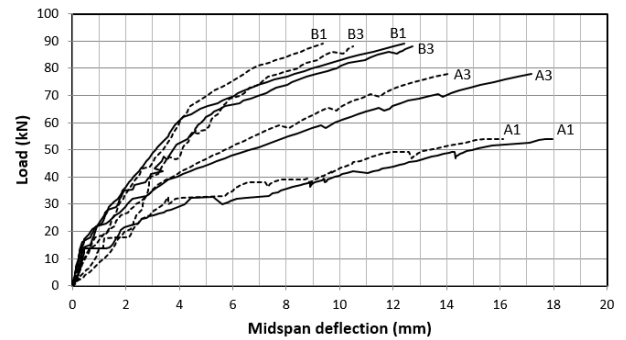


(c) Beam B1 left midspan

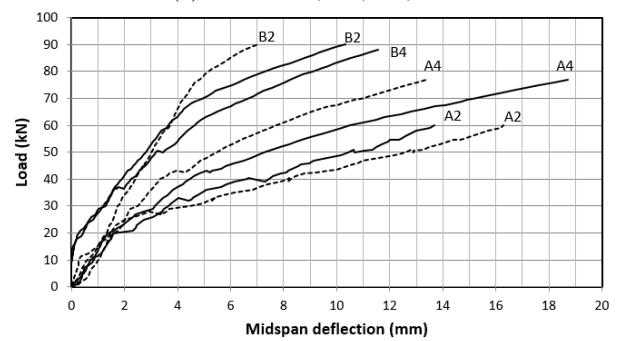
Fig. 4 Crack patterns: Beam A1 left midspan (a); Beam A3 left midspan (b); Beam B1 left midspan (c)

distributions were observed in the tests. During the tests, it was seen that the initial cracks occurred at the mid-support of the specimens and vertical cracks occurred at midspan of the beams. After that, the existing cracks continued to propagate and new cracks also appeared along the beams' length. The cracks were marked on the specimens in the tests. It is seen in Fig. 4 that more cracks occurred along the beam length for the beams reinforced with combinations of GFRP and steel bars (A3, B1) when compared to beam reinforced with pure GFRP bars (A1). In addition, crack width propagation was prevented for the beams including high reinforcement ratio when compared to tested beams including low reinforcement ratio.

The experimental load and corresponding vertical displacements at each midspan were measured during the tests to attain the experimental load-deflection curves of continuous beams. Fig. 5 depicts the experimental load-deflection diagrams using exact values of left and right midspan deflection measurements. The vertical displacement measurements of right midspan of beam B4 were not obtained due to a recording problem during the test. Flexural failure was observed in all the tested beams.



(a) Beams A1, A3, B1, B3



(b) Beams A2, A4, B2, B4

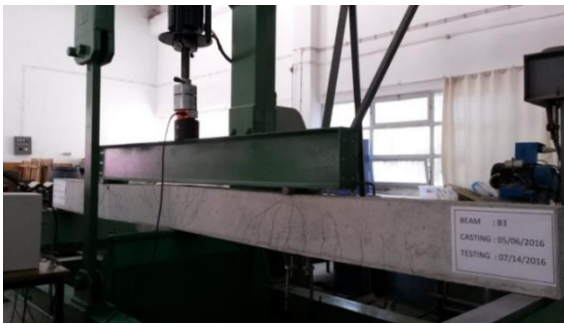
Fig. 5 Experimental load-deflection curves of tested beams: A1, A3, B1, B3 (a); A2, A4, B2, B4 (b)

Flexural cracking was emerged in the tension side of the specimens and the concrete was crushed in the compression side when failure occurred. Over-reinforced design was provided for the beams since the GFRP material exhibited non-ductile behavior. Therefore, as expected, FRP rupture did not occur for the tested beams reinforced with pure GFRP and/or combinations of GFRP and steel bars. Larger deformations were observed for the beams having lower reinforcement ratio. The bending capacity of continuous beams reinforced with combinations of GFRP and steel reinforcement were higher than tested beams reinforced with pure GFRP bars due to including high reinforcement ratio. It was observed from the failure mechanisms that tested beams were appropriately designed in shear. The typical failure mode of beams is presented in Fig. 6.

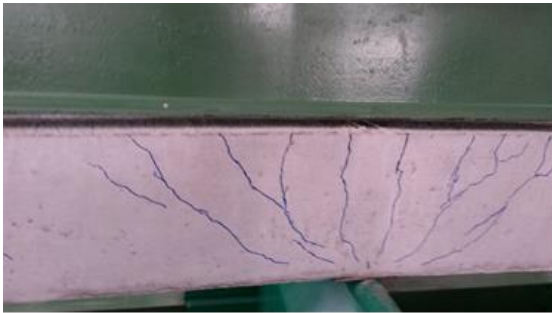
Fig. 5(a) illustrates the load-deflection behavior of beams A1, A3, B1 and B3. Stiffness of four beams change at a cracking load of about 15 kN. Beam stiffness decreased beyond this point due to cracking. Steel yielding occurred at a load of about 40 kN for the beam A3 and 62 kN for the beam B1 and 67 kN for the beam B3.

The specimen A3 demonstrated slightly stiffer response with respect to specimen A1 due to the reinforcement ratio of steel to GFRP. In addition, beams B1 and B3 showed almost the same performance in terms of strength and stiffness.

Fig. 5(b) depicts the load-deflection behavior of beams A2, A4, B2 and B4. Steel yielding occurred at a load of about 45 kN for the beam A4, 62 kN for the beam B4 and 69 kN for the beam B2. Beyond this point, stiffness of



(a) General view



(b) Mid-support



(c) Failure zone at mid-support



(d) Left midspan

Fig. 6 The typical failure mode of beams: General view (a); Mid-support (b); Failure zone at mid-support (c); Left midspan (d)

beams reinforced with GFRP and steel bars decreased due to low modulus of GFRP bars. Placing steel reinforcement at the inner layer of B4 caused a slight drop in the stiffness and the strength of the beam, as expected. The curves of beams A2 and A4 were coincided until about 20 kN. As the stiffness of both beams decreased beyond this point, beam A4 performed stiffer behavior due to the presence of steel bars in the section. This demonstrated the clear contribution of steel reinforcement to stiffness of the beams reinforced with combinations of GFRP and steel bars.

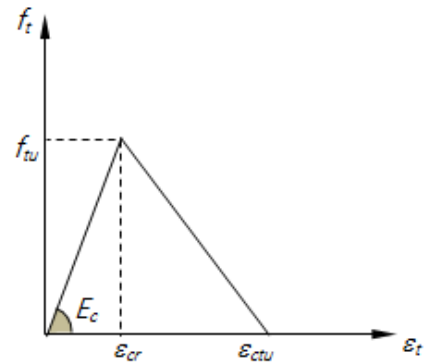


Fig. 7 The stress-strain relationship for concrete in tension

3. Analysis method

A theoretical procedure to analyze the FRP or steel reinforced continuous concrete beams under bending has been previously presented in Dundar *et al.* (2015). In this study, that procedure is extended and modified to achieve the analysis of continuous concrete beams reinforced with combination of FRP and steel bars. The modified procedure in this paper utilizes the stiffness matrix method with a fast incremental/iterative solution algorithm to determine the load-deflection behavior of concrete members reinforced with combination of FRP and steel bars.

The procedure considers effective flexibilities of members in the cracked state using the curvature distribution along the member under any loading or support condition. The initial stage of the analysis calculates moment-curvature relationships of each different section type in the structural system up to the level of ultimate moment capacity. The moment capacity and curvature equations corresponding to a specific deformation are developed using an incremental deformation technique (Kara *et al.* 2013, 2015, Dundar *et al.* 2015).

A bilinear tensile stress-strain model is used for concrete in tension. The model is described with the following equations

$$f_t = E_c \varepsilon_t \quad \varepsilon_t \leq \varepsilon_{cr} \quad (1a)$$

$$f_t = f_r - \frac{f_r}{\varepsilon_{ctu} - \varepsilon_{cr}} (\varepsilon_t - \varepsilon_{cr}), \varepsilon_{ctu} \geq \varepsilon_t \geq \varepsilon_{cr} \quad (1b)$$

$$\varepsilon_{ctu} = \alpha_{ts} \varepsilon_{cr} \quad (1c)$$

where, f_t and ε_t are the tensile stress and strain of the concrete; E_c is the modulus of elasticity of concrete; f_r and ε_{cr} are the modulus of rupture of the concrete and the corresponding cracking strain; and ε_{ctu} is the ultimate tensile strain of the concrete. The parameter α_{ts} is defined as α_{ts} times of the cracking strain (ε_{cr}) as shown in Fig. 7. The value of α_{ts} is taken to be 5 in this study (Prakhya and Morley 1990, Kaklauskas and Ghaboussi 2001, Kara *et al.* 2013, Dundar *et al.* 2015).

CEB-FIB (1990) model is assumed for concrete in compression. The behavior of FRP bars is modeled as linear elastic material up to rupture. The compressive strength of GFRP bars is disregarded in the calculations. The stress-

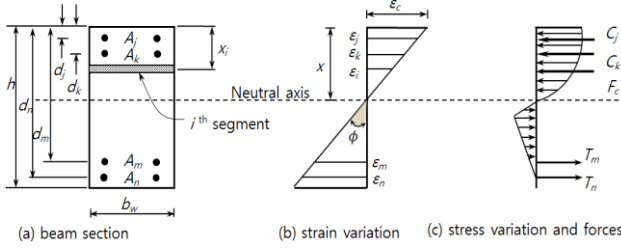


Fig. 8 Strains, stresses and forces of concrete beam cross section reinforced with combination of FRP and steel bars

strain relationship of steel is modeled as an elastic-plastic material. The model equations to represent the material laws were given in Dundar *et al.* (2015).

Fig. 8 shows a reinforced concrete beam section which contains double reinforcement layers with FRP and steel bars in tension and compression zone, strain and stress variations, and the resultant forces. Since the modified numerical procedure was developed to predict the actual behavior of beams in general, the formulations are executed to consider single or double reinforcement layers both in tension and compression zones, with the contents of tension or compression FRP and steel reinforcement bars. In the procedure, the mechanical properties of reinforcement materials such as their tensile yield strength, compressive yield strength, tensile modulus of elasticity and compressive modulus of elasticity are defined separately.

Assuming linear strain distribution over the section, the concrete strain at segment i and strains in the compression and tension reinforcing FRP or steel bars can be expressed as (Fig. 8)

$$\varepsilon_i = \frac{x - x_i}{x} \varepsilon_c; \quad \varepsilon_j \text{ or } \varepsilon_k = \frac{x - (d_j \text{ or } d_k)}{x} \varepsilon_c \quad (2a)$$

$$\varepsilon_m \text{ or } \varepsilon_n = \frac{x - (d_m \text{ or } d_n)}{x} \varepsilon_c \quad (2b)$$

where, x is the depth of neutral axis; x_i is the distance of i -th concrete segment from the most heavily compressed fiber; ε_c denotes the compressive strain at the concrete extreme fiber of the section; ε_i represents the concrete compressive or tensile strain of the i -th segment; ε_j or ε_k is the compressive strain for FRP and steel reinforcing bars in j -th or k -th layer; and ε_m or ε_n denotes the tensile strain for FRP and steel reinforcing bars in m -th or n -th layer; and d_j or d_k indicates the depth of FRP and steel compression reinforcing bars in j -th or k -th layer; and d_m or d_n is the depth of FRP and steel tension reinforcing bars in m -th or n -th layer, respectively.

As shown in Fig. 8, force equilibrium equation can be expressed as follows

$$\sum F = F_c + (C_j + C_k) - (T_m + T_n) = 0 \quad (3a)$$

where, F_c is the resultant concrete force; and C_j and C_k indicate resultant compression force in the FRP and/or steel reinforcement; and T_m and T_n denote resultant tension force in the FRP and/or steel reinforcement, respectively. These forces are determined as follows:

$$F_c = \sum_{i=1}^n f_{ci} h_i b_w \quad (3b)$$

$$C_j = A_j E_j \varepsilon_j \quad C_k = A_k E_k \varepsilon_k \quad (3c)$$

$$T_m = A_m E_m \varepsilon_m \quad T_n = A_n E_n \varepsilon_n \quad (3d)$$

where, f_{ci} represents the concrete compressive or tensile stress at the i -th segment; h_i and b_w indicate the height of the i -th segment and the width of the beam section, respectively; A_j or A_k denotes the total area of FRP and/or steel compression reinforcing bars in j -th or k -th layer; and A_m or A_n is the total area of FRP and/or steel tension reinforcing bars in m -th or n -th layer; and E_j or E_k denotes the modulus of elasticity for FRP and/or steel compression reinforcing bars in j -th or k -th layer; and E_m or E_n represents the modulus of elasticity for FRP and/or steel tension reinforcing bars in m -th or n -th layer, respectively.

After satisfying Eq. (3a) by iterative procedure, the moment-curvature relation of the member is then obtained by the following equations

$$\phi_M = \frac{\varepsilon_c}{x} \quad (4)$$

$$M = \sum_{i=1}^n F_{ci} (x - x_i) + (T_m)(x - d_m) + (T_n)(x - d_n) + (C_j)(x - d_j) + (C_k)(x - d_k) \quad (5)$$

where F_{ci} denotes the concrete compressive or tensile force at middepth of the i -th segment. Although the equations given above are formulated for double layer of tension and/or compression reinforcement, they are also valid for the case of a single layer consisted of FRP and steel reinforcing bars in tension ($d_m = d_n$) and/or in compression ($d_j = d_k$).

Using moment-curvature relationship of a specific section, the effective flexibility of the member is computed with the flexibility equation given in Dundar *et al.* (2015) as follows

$$\frac{1}{E_c I_{eff}} = \frac{1}{E_c I_{cr}} \left[1 - \left(1 - \frac{\phi_M}{M_a} \right) E_c I_{cr} \right] \leq \frac{1}{E_c I_g} \quad (6)$$

where, E_c is the modulus of elasticity of concrete; M_a and M_{cr} denote the applied bending moment and the flexural cracking moment of the section, respectively; I_g is the moment of inertia of gross concrete section about the centroidal axis, I_{cr} is the moment of inertia of cracked section transformed to concrete. Eq. (6) is used to determine the flexibility matrix of the member. Cracked and uncracked regions of the members are determined using the member end forces. The modified procedure initially considers all the members to be uncracked and performs the linear elastic analysis of the structure. The cracked members are then identified and their flexural stiffness ($E_c I_{eff}$) is determined by using moment curvature distributions. The contributions of cracked and uncracked regions to the member flexibility matrix are computed using

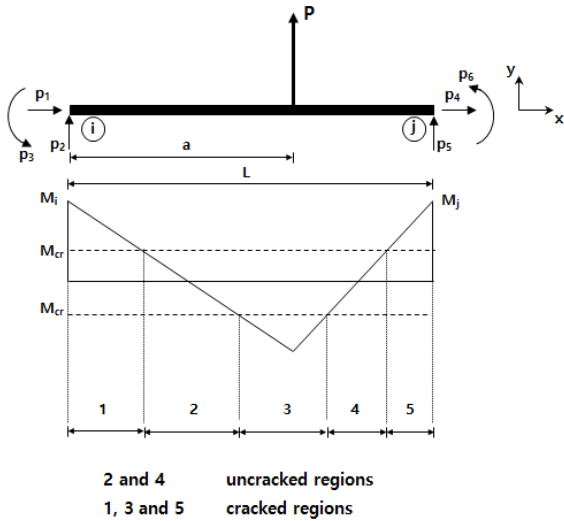


Fig. 9 Cracked and uncracked regions of the member with positive end forces

a numerical integration technique. Cracked and uncracked regions and positive end forces of a member are shown in Fig. 9. Stiffness matrix of cracked member is simply obtained by inverting the flexibility matrix of the member. Structure stiffness matrix equation is assembled and solved for joint displacements and member end forces. The member end forces used at each iteration are taken as the mean value of the end forces of all previous iterations. Iteration is performed until convergence criterion that is given in Eq. (7) is satisfied. This procedure accelerates convergence of the algorithm.

$$\left| \frac{p_i^n - p_i^{n-1}}{p_i^n} \right| \leq \epsilon \quad (7)$$

where ϵ is the convergence factor, n is the iteration number, and p_i^n ($i=1-6$) is the end forces of each member of the structure for the n -th iteration. The iterative procedure is illustrated in the flow chart in Fig. 10. More details of the theoretical analysis procedure can be attained in Dundar *et al.* (2015).

4. Computer analysis of two-span continuous beams

The tested two-span continuous beams were analyzed with the computer program developed based on the modified numerical procedure to determine the theoretical load-deflection curves. The cross-section details and material properties of the beams are presented in Fig. 1 and Table 1.

The predicted and experimental midspan load-deflection curves of the two-span continuously supported beams are illustrated in Figs. 11-18.

As seen in Figs. 13-18, three distinct segments are observed in the load-deflection curves of beams reinforced with combinations of GFRP and steel bars. Reduction in slope indicates a decrease in stiffness of beams due to cracking of concrete and yielding of steel. It is observed in Fig. 11 and Fig. 13 that the load-deflection curves are

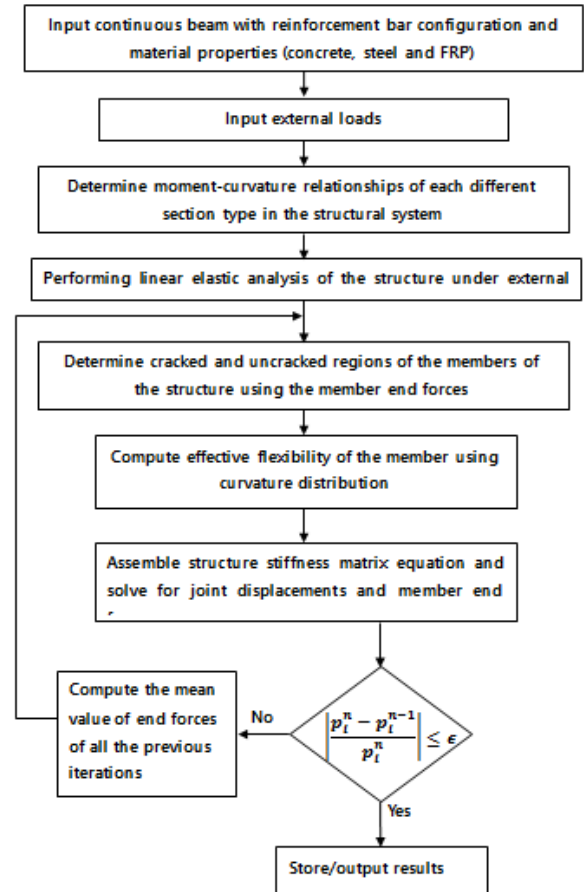


Fig. 10 Flow chart of the algorithm

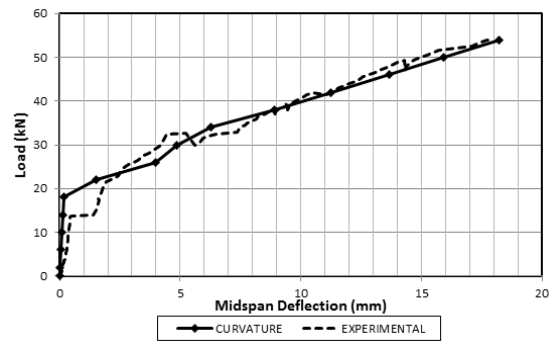


Fig. 11 Experimental and predicted load-deflection relationship of beam A1

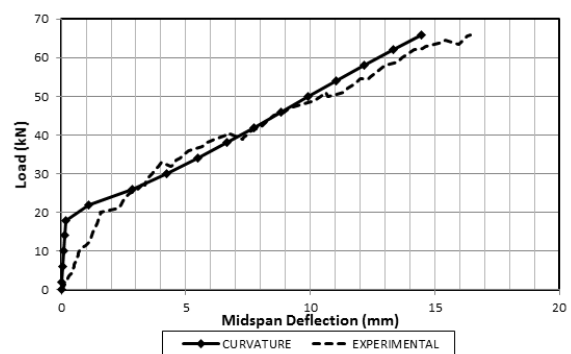


Fig. 12 Experimental and predicted load-deflection relationship of beam A2

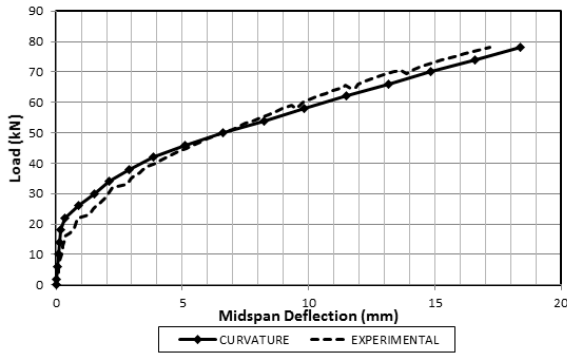


Fig. 13 Experimental and predicted load-deflection relationship of beam A3

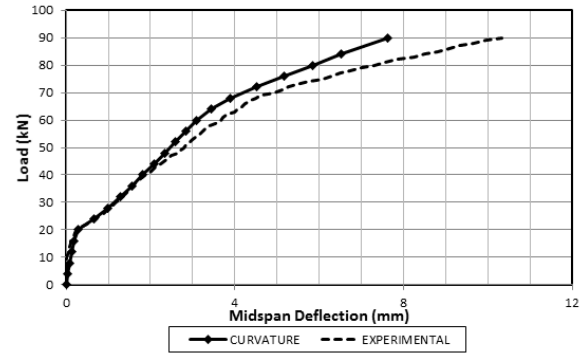


Fig. 16 Experimental and predicted load-deflection relationship of beam B2

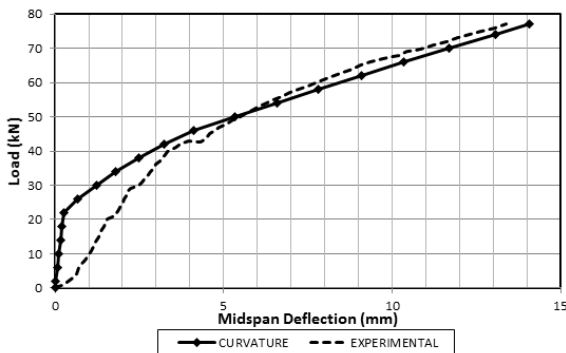


Fig. 14 Experimental and predicted load-deflection relationship of beam A4

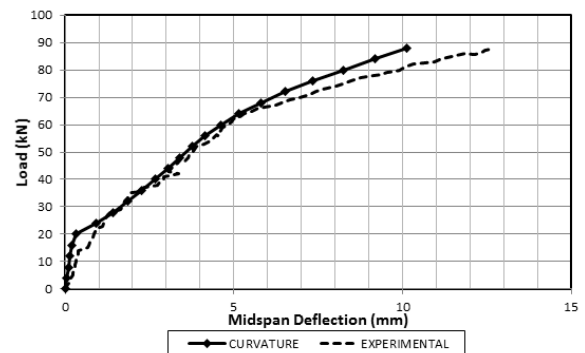


Fig. 17 Experimental and predicted load-deflection relationship of beam B3

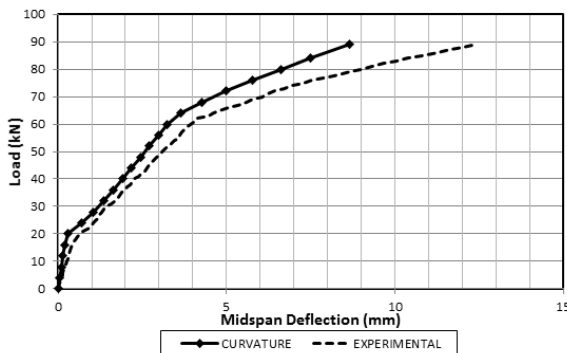


Fig. 15 Experimental and predicted load-deflection relationship of beam B1

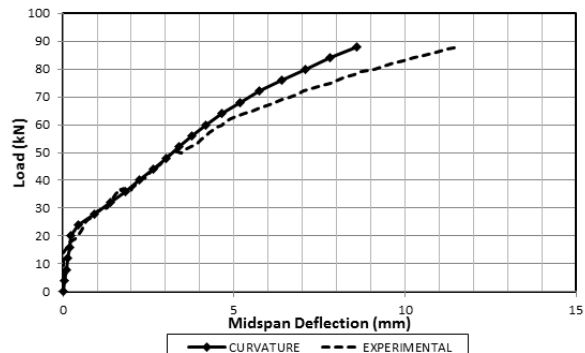


Fig. 18 Experimental and predicted load-deflection relationship of beam B4

obtained in good agreement from zero to ultimate load for the beams A1 and A3. On the other hand, the experimental and the theoretical curves for beams A2 and A4 exhibit dissonant behavior from zero to cracking load in the study. Beyond this point, there is good agreement between the experimental and predicted curves up to the ultimate load (Fig. 12 and Fig. 14).

It is seen in Figs. 15-18 that, the numerical load-deflection curves of the beams B1, B2, B3 and B4 are compare well with the test results from zero to steel yielding load. However, the numerical predictions provide a slightly stiffer response from the load corresponding to yielding of steel to ultimate load. This can be explained that the analytical curves represent homogenized load-deflection

responses, on the other hand experimental curves represent localized responses that depend on a primary crack.

5. Conclusions

A total of eight two-span concrete beams reinforced with pure GFRP bars and combinations of GFRP and steel bars were prepared and tested in this study. The specimens were manufactured with different reinforcement configurations. The beams were tested subject to static loading condition. The experimental load-deflection diagrams, crack distribution and failure mode of the specimens were observed in the study. Rupture of GFRP bar

was prevented by over-reinforcement design. The reinforcement configuration with pure GFRP bars and combinations of GFRP and steel reinforcement differed on deformation capacity of continuous beams. Larger deformations were seen for the beams having lower reinforcement ratio.

The tested continuous beams reinforced with pure GFRP bars and combinations of GFRP and steel bars were analyzed by using the computer program developed based on the theoretical procedure. The reinforcement design, flexural tensile strength and compressive strength of concrete, yield strength and modulus of elasticity of reinforcement parameters were taken into account in the analysis. The findings revealed that the predicted load-deflection curves obtained based on the numerical procedure is in good agreement with the experimental results in the study.

Acknowledgements

The presented research study was financially supported by Cukurova University Scientific Research Projects Directorate (Project No. FDK-2015-4924). The experimental work was assisted by Cukurova University laboratory staffs. The authors would like to thank for these contributions.

References

- ACI 440.1R-15 (2015), Guide for the design and construction of structural concrete reinforced with FRP bars, American Concrete Institute, Farmington Hills, MI, USA.
- Adam, M.A., Said, M., Mahmoud, A.A. and Shanour, A.S. (2015), "Analytical and experimental flexural behavior of concrete beams reinforced with glass fiber reinforced polymer bars", *Constr. Build. Mater.*, **84**, 354-66.
- Bencardino, F., Condello, A. and Ombres, L. (2016), "Numerical and analytical modelling of concrete beams with steel, FRP and hybrid FRP-steel reinforcements", *Compos. Struct.*, **140**, 53-65.
- Bischoff, P.H. (2007), "Deflection calculation of FRP reinforced concrete beams based on the modifications to the existing Branson equation", *J. Compos. Constr.*, **11**(1), 4-14.
- CAN/CSA-S806-12 (2012), Design and construction of building structures with fiber reinforced polymers, CSA.
- Comité Euro-International du Béton (CEB) (1990), CEB-FIB model for concrete structures, Bulletin 213/214.
- Dundar, C., Tanrikulu, A.K. and Frosch, R.J. (2015), "Prediction of load-deflection behavior of multi-span FRP and steel reinforced concrete beams", *Compos. Struct.*, **132**, 680-93.
- Elamary, A.S. and Abd-Elwahab, R.K. (2016), "Numerical simulation of concrete beams reinforced with composite GFRP-Steel bars under three points bending", *Struct. Eng. Mech.*, **57**(5), 937-949.
- Elgabbas, F., Vincent, P., Ahmed, E.A. and Benmokrane, B. (2016), "Experimental testing of basalt-fiber-reinforced polymer bars in concrete beams", *Compos. Part B*, **91**, 205-218.
- Goldstone, M., Remennikov, A. and Sheikh, M.N. (2016), "Experimental investigation of the behaviour of concrete beams reinforced with GFRP bars under static and impact loading", *Eng. Struct.*, **113**, 220-32.
- Gribniak, V., Caldentey, A.P., Kaklauskas, G. and Rimkus, A. (2016), "Effect of arrangement of tensile reinforcement on flexural stiffness and cracking", *Eng. Struct.*, **24**, 418-428.
- Kaklauskas, G. and Ghaboussi, J. (2001), "Stress-strain relations for cracked tensile concrete from RC beam tests", *J. Struct. Eng.*, **127**(1), 63-73.
- Kara, I.F. (2016), "Flexural performance of FRP-reinforced concrete encased steel composite beams", *Struct. Eng. Mech.*, **59**(4), 775-793.
- Kara, I.F. and Ashour, A.F. (2012), "Flexural performance of FRP reinforced concrete beams", *Compos. Struct.*, **94**, 1616-1625.
- Kara, I.F. and Dundar, C. (2012), "Prediction of deflection of high strength steel fiber reinforced concrete beams and columns", *Comput. Concrete*, **9**(2), 133-151.
- Kara, I.F., Ashour, A.F. and Dundar, C. (2013), "Deflection of concrete structures reinforced with FRP bars", *Compos: Part B*, **44**, 375-384.
- Kara, I.F., Ashour, A.F. and Koroglu, M.A. (2015), "Flexural behavior of hybrid FRP/steel reinforced concrete beams", *Compos. Struct.*, **129**, 111-121.
- Lou, T., Lopes, S.M.R. and Lopes, A.V. (2015), "Neutral axis depth and moment redistribution in FRP and steel reinforced concrete continuous beams", *Compos. Part B*, **70**, 44-52.
- Maranan, G.B., Manola, A.C., Benmokrane, B., Karunasena, W. and Mendis P. (2015), "Evaluation of the flexural strength and serviceability of geopolymer concrete beams reinforced with glass-fibre-reinforced polymer (GFRP) bars", *Eng. Struct.*, **101**, 529-41.
- Mazaheripour, H., Barros, J.A.O., Soltanzadeh, F. and Sena-Cruz, J. (2016), "Deflection and cracking behavior of SFRSCC beams reinforced with hybrid prestressed GFRP and steel reinforcements", *Eng. Struct.*, **125**, 546-565.
- Mohamed, N., Farghaly, A.S. and Benmokrane, B. (2016), "Beam-testing method for assessment of bond performance of FRP bars in concrete under tension-compression reversed cyclic loading", *J. Compos. Constr.*, 06016001.
- Prakhya, G.K.V. and Morley, C.T. (1990), "Tension stiffening and moment-curvature relations for reinforced concrete elements", *ACI Struct. J.*, **87**(5), 597-605.
- Qin, R., Zhou, A. and Lau, D. (2017), "Effect of reinforcement ratio on the flexural performance of hybrid FRP reinforced concrete beams", *Compos. Part B*, **108**, 200-209.
- Qu, W., Zhang, X. and Huang, H. (2009), "Flexural behavior of concrete beams reinforced with hybrid GFRP and steel bars", *J. Compos. Constr.*, ASCE, **13**(5), 350-359.
- Refai, A.E., Abed, F. and Al-Rahmani, A. (2015), "Structural performance serviceability of concrete beams reinforced with hybrid (GFRP and steel) bars", *Constr. Build. Mater.*, **96**, 518-529.
- Tanrikulu, A.K., Dundar, C. and Cagatay, I.H. (2000), "A computer program for the analysis of reinforced concrete frames with cracked beam elements", *Struct. Eng. Mech.*, **10**(5), 463-78.
- Thomas, J. and Ramadass, S. (2015), "Design for shear strength of concrete beams longitudinally reinforced with GFRP bars", *Struct. Eng. Mech.*, **53**(1), 41-45.
- Yinghao, L. and Yong, Y. (2013), "Arrangement of hybrid rebars on flexural behavior of HSC beams", *Compos. Part B*, **55**, 22-31.
- Zhang, L., Sun, Y. and Xiong, W. (2015), "Experimental study on the flexural deflections of concrete beam reinforced with Basalt FRP bars", *Mater. Struct.*, **48**, 3279-3293.
- Zhao, X.L. and Zhang, L. (2007), "State-of-the-art review on FRP strengthened steel structures", *Eng. Struct.*, **29**, 1808-23.